I&EC research
Industrial & Engineering Chemistry Research

pubs.acs.org/IECR

Article

Assessment of Modeling the MgO-CaO-CO_2-SO_2-H_2O-O_2 System Using the Electrolyte NRTL Activity Coefficient Model

Barbara D. Weiß, Bahram Haddadi,* and Michael Harasek

Cite This: https://doi.org/10.1021/acs.iecr.3c00868

Read Online

ACCESS | Metrics & More | Article Recommendations

ABSTRACT: This work assesses the thermodynamic modeling of the MgO-CaO-CO_2-SO_2-H_2O-O_2 system using the electrolyte NRTL activity coefficient model, primarily focusing on the solubility of potential salts in the system. The assessment includes the SO_2-H_2O and SO_2-$Mg(OH)_2$ vapor−liquid equilibria as well as the precipitation of $Mg(OH)_2$, $Ca(OH)_2$, $MgSO_3$, $CaSO_3$, $MgSO_4$, $CaSO_4$, and their hydrate forms. The analysis covers a temperature range of 0 to 100 °C and focuses on calculations at atmospheric pressure. The performed calculations assess the necessity of defining equilibrium constants K_{eq} as a function of temperature to describe the chemical equilibria accurately. The SO_2 solubility in water is studied for a pressure range of 0.545 to 1.788 bar. The SO_2-$Mg(OH)_2$ absorption equilibrium is studied for a SO_2 partial pressure range of 0.00963 to 1.101325 bar and a MgO concentration of up to 14.5 kg/m^3 H_2O. The results are evaluated using experimentally determined data from the literature. The study shows that the model recognizes all reported precipitation forms in the correct temperature range in chemically stable systems. The solubility of $Mg(OH)_2$ is calculated with a deviation from literature data of <6% for a temperature range of 70 to 90 °C and a maximum deviation of −40% for temperatures close to 0 °C. The calculated $Ca(OH)_2$ solubility at the complete studied temperature range deviates less than 11% from the literature data. The model also recognizes the pH dependency of the solubility of both hydroxides. The calculated solubility of $MgSO_3$ hexahydrate deviates less than 1% from literature data, and the calculated solubility of $MgSO_3$ trihydrate shows a maximum deviation from literature data of 20% at temperatures up to 90 °C. The solubility of $CaSO_3$ hemihydrate is predicted with a deviation of <1% at a temperature range of 70 to 100 °C and a deviation of <30% for temperatures higher than 20 °C. The model predicts the solubility of $MgSO_4$ monohydrate with a maximum deviation from literature data of 20% and overestimates the solubility of $MgSO_4$ heptahydrate by up to 118% compared to literature data. The solubility of $CaSO_4$ monohydrate is calculated with a deviation from literature data of <2%, and the solubility of $CaSO_4$ dihydrate with a deviation of <7%. The model's accuracy in predicting the SO_2 solubility in water variates strongly depending on which literature data points it is compared to. The smallest deviation from literature data is 1% compared to data measured at 60 °C and a pressure of 1.377 bar. The highest deviation is 60% compared to data measured at 90 °C and atmospheric pressure. The study shows that the experimental data in literature describing the SO_2 absorption in an $Mg(OH)_2$ solution are scarce. This leads to a limited ability to evaluate thermodynamic models based on experimental data. The model describes the SO_2 absorption in $Mg(OH)_2$ with a deviation between 8 and 52% compared to available literature data.

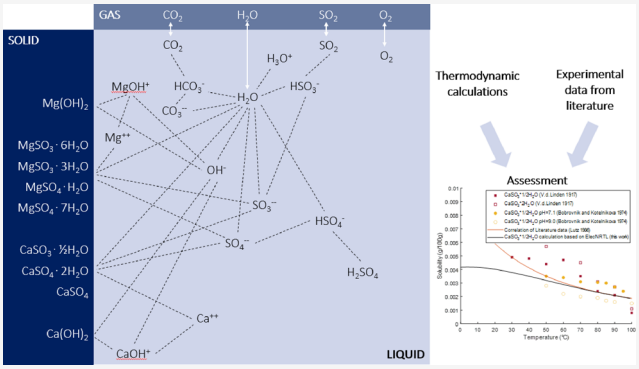

1. INTRODUCTION

The MgO-CaO-CO_2-SO_2-H_2O-O_2 system is an important electrolyte system for flue gas treatment processes, where SO_2 is removed from the gas by absorption. It has particular importance in the pulp and paper industry, as the absorption of SO_2 using $Mg(OH)_2$ slurry allows the recovery of magnesium bisulfite, which then can be used as cooking liquor for pulp production again. The absorption of SO_2 using magnesium hydroxide slurry has recently gained increased attention due to the possibility of removing pollutants SO_2 and NO_x simultaneously.[1] Complex industrial absorption processes often have up to 10 absorption steps. To run the process in an optimized way, mechanistic models are of great importance. A mechanistic model allows a deeper understanding of the complex electrolyte system and the detection of critical zones in the process chain. A mechanistic model combined with process control data of a

Received: March 16, 2023
Revised: July 14, 2023
Accepted: July 20, 2023

plant can provide a digital twin of the plant, which can be used to find optimized process parameters or to control the process.

The MgO-CaO-CO_2-SO_2-H_2O-O_2 system is prone to precipitation in the system. While in some processes, precipitation is wanted to separate the solids from the liquid, in the chemical recovery of the pulp industry, precipitation is highly undesired. Uncontrolled precipitation causes the blockage of pipes and consequential chemical loss.[2] Whether the precipitation is desired or avoided, a rigorous thermodynamic model can serve as a valuable tool to identify precipitation in the system. The occurrence of precipitation depends on the complex present electrolyte system. Therefore, a mechanistic model needs to cover all relevant reactions of that system.

The electrolyte NRTL model is a commonly used method to model electrolyte systems. Si et al. applied the electrolyte NRTL method to an SO_2 absorption system based on calcium.[3] Schöggl et al. described the MgO-H_2O-SO_2 system using the electrolyte NRTL method.[4] Their study indicates that the method is applicable to model that system. However, the study also suggests improving the model by adapting the calculation results to literature data through an external function that overwrites the calculation results with input data. Zidar et al. modeled the MgO-H_2O-SO_2 equilibrium using the Rudzinski+Pitzer-Ion activity coefficient model.[5] They used the Pitzer's ion interaction model to calculate the activity coefficients in the mixture and the Rudzinski method to determine the pH value. While there are earlier studies available building up to the results of Zidar et al.,[6] there are no newer studies found in literature that target the topic of thermodynamic modeling of the absorption system. The lack of available studies motivated the authors to conduct a comprehensive assessment of the applicability of the semi-empirical electrolyte NRTL method to model the absorption equilibrium as well as precipitations in the system. This study evaluates the applicability of the electrolyte NRTL method to model the SO_2 absorption using up-to-date available thermodynamic property data and the solubility of all potential salts in the system. The calculated results are compared to available experimental data from the literature.

2. METHODS

The system was rigorously modeled using the simulation environment and data banks of Aspen Plus V10. The electrolyte system is described using the true component approach. The true component approach, unlike the apparent component approach, means that all true components of the electrolyte system, including ions, salts, and molecular species, are reported. The results were evaluated using literature data reviewed in a previous study.[7] The following summarizes the applied methodology.

2.1. Thermodynamic Framework. The electrolyte NRTL activity coefficient model was applied as proposed by Chen and Evans and extended by Mock et al.[8,9] The vapor phase properties were calculated using the Redlich−Kwong equation of state.[10]

The system was calculated in phase equilibrium. The equality of the fugacity of every component in the different present phases is the basis of the performed key thermodynamic property calculations:

$$f_i^{\mathrm{v}} = f_i^{\mathrm{l}} \tag{1}$$

2.1.1. Vapor Phase Properties—Redlich−Kwong Equation of State. The fugacity of the vapor phase is expressed as follows:

$$f_i^{\mathrm{v}} = \varphi_i^{\mathrm{v}} y_i p \tag{2}$$

The fugacity coefficients are represented by

$$\ln \varphi_i^{\mathrm{v}} = -\frac{1}{RT} \int_{\infty}^{V^{\mathrm{v}}} \left[\left(\frac{\partial p}{\partial n_i} \right)_{T,V,n_{j\neq i}} - \frac{R}{TV} \right] \mathrm{d}V - \ln Z_{\mathrm{m}}^{\mathrm{v}} \tag{3}$$

with

$$Z_{\mathrm{m}}^{\mathrm{v}} = \frac{pV}{nRT} \tag{4}$$

The vapor phase properties are calculated by the cubic equation of state Redlich−Kwong:[10]

$$p = \frac{RT}{V_{\mathrm{m}} - b} - \frac{\frac{a}{\sqrt{T}}}{V_{\mathrm{m}}(V_{\mathrm{m}} + b)} \tag{5}$$

$$\sqrt{a} = \sum_i y_i \sqrt{a_i} \tag{6}$$

$$b = \sum_i y_i b_i \tag{7}$$

$$a_i = 0.42748023 \frac{R^2 T_{ci}^{2.5}}{p_{ci}} \tag{8}$$

$$b_i = 0.08664 \frac{RT_{ci}}{p_{ci}} \tag{9}$$

The critical temperature and the critical pressure of the pure components were retrieved from the standard implemented data banks in Aspen Plus V10.

2.1.2. Liquid Phase Properties—Electrolyte NRTL Activity Coefficient Model. The fugacity of the liquid phase is expressed as follows:

$$f_i^{\mathrm{l}} = f_i^{*,\mathrm{l}} x_i \gamma_i \tag{10}$$

$$f_i^{*,\mathrm{l}} = F_{p,i}^{*} \varphi_i^{*,\mathrm{v}} p_i^{*} \tag{11}$$

$$F_{p,i}^{*} = \mathrm{e}^{1/RT \int_{p_i^{*}}^{p} V_{\mathrm{m}i}^{*,\mathrm{l}} \mathrm{d}p} \tag{12}$$

The activity coefficient represents the deviation of the mixture from ideality. The reference state defines which state is referred to as ideal. In other words, the reference state dictates the conditions at which the activity coefficient is assigned to the value of 1.[11] The properties of the reference state are denoted by *. For supercritical components (CO_2, O_2, and SO_2) and ions, the model was calculated using an unsymmetric reference state, which means that the reference state is at infinite dilution at system temperature and pressure:

$$\gamma_i^{*} = \frac{\gamma_i}{\gamma_i^{\infty}} \tag{13}$$

The basis for the unsymmetric activity coefficient is the actual mixed solvent present. For all other components, the reference state is that of a pure compound. The liquid phase reference fugacity is then defined as that of the pure liquid component *i* at system temperature and pressure.

https://doi.org/10.1021/acs.iecr.3c00868
Ind. Eng. Chem. Res. XXXX, XXX, XXX−XXX

The behavior of dissolved gases, such as CO_2, O_2, and SO_2, is represented using Henry's law. The expression of the fugacity of the liquid phase becomes the following:

$$f_i^{\mathrm{l}} = H_i x_i \gamma_i^* \tag{14}$$

The temperature-dependent Henry's constants were retrieved from the standard implemented data banks in Aspen Plus V10. Table 1 gives the applied $\ln(H)$ exemplary for 70 °C.

Table 1. Applied Henry's Constants Expressed as $\ln(H_{ij})$ at 70 °C

component i	component j	$\ln(H_{ij})_{T=70°C}$
SO_2	H_2O	4.91122046
O_2	H_2O	−18.0625181
CO_2	H_2O	8.26167044

The activity coefficients were calculated using the electrolyte NRTL activity coefficient model.[8,9] The model is based on the assumptions that, due to strong repulsive forces between ions of like charge, the immediate neighbors of any ions are ions of opposite charge and that the distribution of ions results in local electroneutrality.

The model describes the excess Gibbs energy based on the following relation:

$$\ln \gamma_i = \left(\frac{\partial \left(n_{\mathrm{total}} \frac{G^{\mathrm{E}}}{RT} \right)}{\partial n_i} \right)_{T,P,n_i} \tag{15}$$

The model describes the activity coefficient with a Pitzer–Debye–Hückel (PDH) and a Born (Born) expression for long-range electrostatic interactions and an NRTL-local composition contribution (lc) for the short-range interactions:

$$\ln \gamma_i = \ln \gamma_i^{\mathrm{PDH}} + \ln \gamma_i^{\mathrm{Born}} + \ln \gamma_i^{\mathrm{lc}} \tag{16}$$

$$\ln \gamma_i^{\mathrm{PDH}} = -\sqrt{\frac{1000}{M_s}} A_\varphi \left[\left(\frac{2 z_i^2}{\rho} \right) \ln(1 + \rho \sqrt{I_x}) + \frac{z_i^2 \sqrt{I_x} - 2\sqrt{I_x^3}}{1 + \rho \sqrt{I_x}} \right] \tag{17}$$

$$A_\varphi = \frac{1}{3} \sqrt{\frac{2\pi N_A d_s}{1000}} \sqrt[3]{\frac{Q_e^2}{\varepsilon_s k T}} \tag{18}$$

$$I_x = \frac{1}{2} \sum x_i z_i^2 \tag{19}$$

$$\ln \gamma_i^{\mathrm{Born}} = \frac{Q_e^2}{2kT} \left(\frac{1}{\varepsilon_s} - \frac{1}{\varepsilon_w} \right) \frac{z_i^2}{r_i} 10^{-2} \tag{20}$$

$$\ln \gamma_i^{\mathrm{lc}} = \frac{\sum_j x_i \tau_{ji} G_{ji}}{\sum_k x_k G_{ki}} + \sum_j \frac{x_j G_{ji}}{\sum_k x_k G_{kj}} \left(\tau_{ji} - \frac{\sum_m x_m \tau_{mj} G_{mj}}{\sum_k x_k G_{kj}} \right) \tag{21}$$

$$G_{ij} = e^{-\alpha_{ij} \tau_{ij}} \tag{22}$$

$$\tau_{ij} = a_{ij} + \frac{b_{ij}}{T} + e_{ij} \ln(T) + f_{ij} T \tag{23}$$

Table 2. Considered Electrolyte System

reaction	type
$2\ H_2O \leftrightarrow OH^- + H_3O^+$	partial dissociation equilibrium
$2\ H_2O + SO_2 \leftrightarrow H_3O^+ + HSO_3^-$	partial dissociation equilibrium
$H_2O + HSO_3^- \leftrightarrow H_3O^+ + SO_3^{--}$	partial dissociation equilibrium
$H_2SO_4 + H_2O \leftrightarrow H_3O^+ + HSO_4^-$	partial dissociation equilibrium
$H_2O + HSO_4^- \leftrightarrow H_3O^+ + SO_4^{--}$	partial dissociation equilibrium
$MgOH^+ \leftrightarrow OH^- + Mg^{++}$	partial dissociation equilibrium
$CaOH^+ \leftrightarrow OH^- + Ca^{++}$	partial dissociation equilibrium
$2\ H_2O + CO_2 \leftrightarrow H_3O^+ + HCO_3^-$	partial dissociation equilibrium
$H_2O + HCO_3^- \leftrightarrow H_3O^+ + CO_3^{--}$	partial dissociation equilibrium
$Mg(OH)_2 \rightarrow OH^- + MgOH^+$	complete dissociation
$Ca(OH)_2 \rightarrow OH^- + CaOH^+$	complete dissociation
$MgSO_4 \rightarrow Mg^{++} + SO_4^{--}$	complete dissociation
$MgSO_3 \rightarrow Mg^{++} + SO_3^{--}$	complete dissociation
$CaSO_4 \rightarrow Ca^{++} + SO_4^{--}$	complete dissociation
$CaSO_3 \rightarrow Ca^{++} + SO_3^{--}$	complete dissociation
$MgCO_3 \rightarrow Mg^{++} + CO_3^{--}$	complete dissociation
$CaCO_3 \rightarrow Ca^{++} + CO_3^{--}$	complete dissociation
$Mg(OH)_2\ (s) \leftrightarrow OH^- + MgOH^+$	salt precipitation equilibrium
$Ca(OH)_2\ (s) \leftrightarrow OH^- + CaOH^+$	salt precipitation equilibrium
$MgSO_3 * 6\ H_2O\ (solid) \leftrightarrow Mg^{++} + SO_3^{--} + 6\ H_2O\ (aqueous)$	salt precipitation equilibrium
$MgSO_3 * 3\ H_2O\ (solid) \leftrightarrow Mg^{++} + SO_3^{--} + 3\ H_2O\ (aqueous)$	salt precipitation equilibrium
$CaSO_3 * {}^1/_2\ H_2O\ (solid) \leftrightarrow Ca^{++} + SO_3^{--} + {}^1/_2\ H_2O\ (aqueous)$	salt precipitation equilibrium
$MgSO_4 * H_2O\ (solid) \leftrightarrow Mg^{++} + SO_4^{--} + 1\ H_2O\ (aqueous)$	salt precipitation equilibrium
$MgSO_4 * 7\ H_2O\ (solid) \leftrightarrow Mg^{++} + SO_4^{--} + 7\ H_2O\ (aqueous)$	salt precipitation equilibrium
$CaSO_4 * 2\ H_2O\ (solid) \leftrightarrow Ca^{++} + SO_4^{--} + 2\ H_2O\ (aqueous)$	salt precipitation equilibrium
$CaSO_4\ (solid) \leftrightarrow Ca^{++} + SO_4^{--}\ (aqueous)$	salt precipitation equilibrium

https://doi.org/10.1021/acs.iecr.3c00868
Ind. Eng. Chem. Res. XXXX, XXX, XXX−XXX

Table 3. Applied Equilibrium Constants Expressed as $\ln(K_{eq})$ at 70 °C

reaction	$\ln(K)_{T=70°C}$
$2\ H_2O \leftrightarrow OH^- + H_3O^+$	−37.510985
$2\ H_2O + SO_2 \leftrightarrow H_3O^+ + HSO_3^-$	−9.31441704
$H_2O + HSO_3^- \leftrightarrow H_3O^+ + SO_3^{--}$	−21.4048358
$MgSO_3 * 6\ H_2O$ (solid) $\leftrightarrow Mg^{++} + SO_3^{--} + 6\ H_2O$ (aqueous)	−15.6969191
$MgSO_3 * 3\ H_2O$ (solid) $\leftrightarrow Mg^{++} + SO_3^{--} + 3\ H_2O$ (aqueous)	−16.7808349
$MgSO_4 * H_2O$ (solid) $\leftrightarrow Mg^{++} + SO_4^{--} + 1\ H_2O$ (aqueous)	−12.3224139
$MgSO_4 * 7\ H_2O$ (solid) $\leftrightarrow Mg^{++} + SO_4^{--} + 7\ H_2O$ (aqueous)	−13.1206858
$CaSO_4 * 2\ H_2O$ (solid) $\leftrightarrow Ca^{++} + SO_4^{--} + 2\ H_2O$ (aqueous)	−18.4221215

$$\alpha_{ij} = c_{ij} + d_{ij}(T - 273.15K) \tag{24}$$

The adjustable parameters—born radius, the dielectric constant coefficients, and the binary interaction parameters—were retrieved from the standard implemented data banks in Aspen Plus V10.

2.1.3. Chemical System. The model includes partial dissociation equilibrium reactions, complete dissociations reactions, and salt precipitation equilibrium reactions. Table 2 summarizes all considered reactions.

The chemical equilibrium is calculated using built-in or user-supplied parameters to describe the equilibrium constants K_{eq} as a function of temperature. If no equilibrium constants are given, the equilibrium is calculated from the reference state Gibbs free energies of the participating components following:

$$\ln(K) = \frac{\Delta G_m^*}{RT} \tag{25}$$

The applied parameters to describe the temperature-dependent equilibrium constants are retrieved from the Aspen Plus V10 data bank. Table 3 gives the applied $\ln(K)$ exemplary for 70 °C.

2.2. Performed Analyses for Assessment. To assess the accuracy of the thermodynamic calculations, the calculated properties were compared with experimental data retrieved from the literature. The deviation of the calculated value from literature data is given as

$$\text{deviation}\ (\%) = \frac{(x_{\text{calculated}} - x_{\text{literature}})}{x_{\text{literature}}} \times 100 \tag{26}$$

The following summarizes the performed calculations and the referenced literature data.

2.2.1. Solubility of SO_2. The solubility of SO_2 in water was calculated following two different approaches. First, it was calculated solely using Henry's Law without any electrolyte reactions. Then, it was calculated considering electrolyte reactions (see 2.1) to evaluate the influence of including the electrolyte equilibrium on the calculated SO_2 solubility. The solubility was calculated for a temperature range from 20 to 90 °C and a pressure range from 0.545 to 1.788 bar. The calculations were compared to experimental data from Rumpf and Maurer and Young et al.[12,13]

2.2.2. SO_2 Absorption in $Mg(OH)_2$ Solution. The SO_2 absorbed in $Mg(OH)_2$-H_2O solution was calculated considering all electrolyte reactions given in 2.1. The calculation was performed to be comparable to available experimental literature data. In the experimental data, the temperatures range from 24 to 29.85 °C and the SO_2 partial pressures from 0.0095 to 0.888 atm. The MgO concentration in water ranges from 0 to 14.5 kg/m^3. The quantitative effect of the presence of $Mg(OH)_2$ on the solubility of SO_2 is expressed as enhancement factor. The enhancement factor describes the increase in solubility of SO_2 when $Mg(OH)_2$ is present in the solution compared to the solubility in pure water. The calculations were compared to experimental data from Mondal and Young et al.[13,14]

2.2.3. Solubility of $Mg(OH)_2$ and $Ca(OH)_2$. Two dissociation reactions describe the solubility of the hydroxides: the dissociation of $Mg(OH)_2$ or $Ca(OH)_2$ and the formation of the ion pair $MgOH^+$ or $CaOH^+$. This makes the solubility of the hydroxides strongly pH-dependent. This dependency is better described by calculating the equilibrium from the reference state Gibbs free energies of the participating components rather than from equilibrium constants. Therefore, the equilibrium was described by the reference state Gibbs free energy calculations. The solubility of $Mg(OH)_2$ and $Ca(OH)_2$ was calculated for a temperature range from 0 to 100 °C and a pH range from 7 to 13. The pH was adjusted by adding HCl to the system, as HCl does not affect the equilibrium equations of the chemical system. To evaluate the influence of modeling the formation of the $MgOH^+$ or $CaOH^+$ ion pair on the calculated solubility, the calculation was performed with and without considering its formation. The calculations were compared to experimental data from Dupré and Bialas, Remy and Kuhlmann, Busch, Whipple and Mayer, Hostetler, Einaga, Lambert and Clever, Dongdong et al., Scholz and Kahlert, Bassett and Taylor, Yeatts and Marshall, Bates et al., and Cameron and Robinson.[15−27]

2.2.4. Solubility of $MgSO_3$ and $CaSO_3$ Hydrates. The solubility of $MgSO_3$ and $CaSO_2$ hydrates was calculated for a temperature range from 0 to 100 °C. The chemical equilibrium was first calculated by the reference state Gibbs free energy calculations and then by applying equilibrium constants (see Table 3). Literature studies report a solubility dependency of $MgSO_3$ and $CaSO_3$ hydrates on the presence of sulfate. Therefore, the influence of $MgSO_4$ or $CaSO_4$ on the solubility was calculated. The calculations were compared to experimental data from Lowell et al., Hagisawa, Markant et al., Söhnel and Rieger, Nývlt, Lutz, van der Linden, Bobrovnik and Kotelnikova, and Bichowsky.[28−36]

2.2.5. Solubility of $MgSO_4$ and $CaSO_4$ Hydrates. The solubility of $MgSO_4$ and $CaSO_4$ hydrates was calculated for a temperature range from 0 to 100 °C. The chemical equilibrium was first calculated by the reference state Gibbs free energy calculations and then by applying equilibrium (see Table 3). The calculations were compared to experimental data from Zhang et al., Robson, Apelblat and Manzurola, Ting and McCabe, Wu et al., Patridge and White, Power and Fabuss, Wang et al., Hulett and Allen, Yuan et al., and Li and Demopoulos.[37−47]

3. RESULTS AND DISCUSSION

The following summarizes and discusses the results of the performed calculations including the SO_2 solubility in water, the SO_2 absorption in $Mg(OH)_2$, the solubility of $MG(OH)_2$ and

https://doi.org/10.1021/acs.iecr.3c00868
Ind. Eng. Chem. Res. XXXX, XXX, XXX−XXX

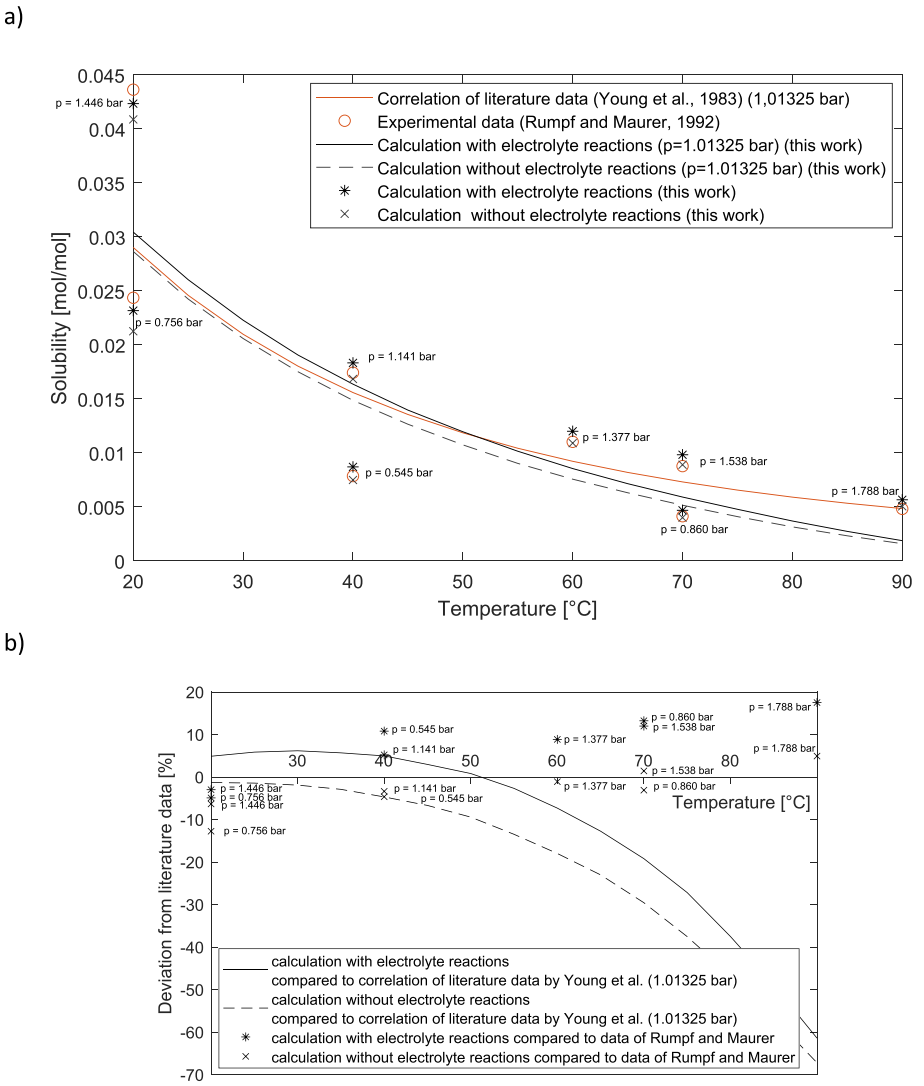

Figure 1. (a) SO_2 solubility in water over temperature at different pressures.[12,13] (b) Deviation of calculated values from literature data (see eq 26).

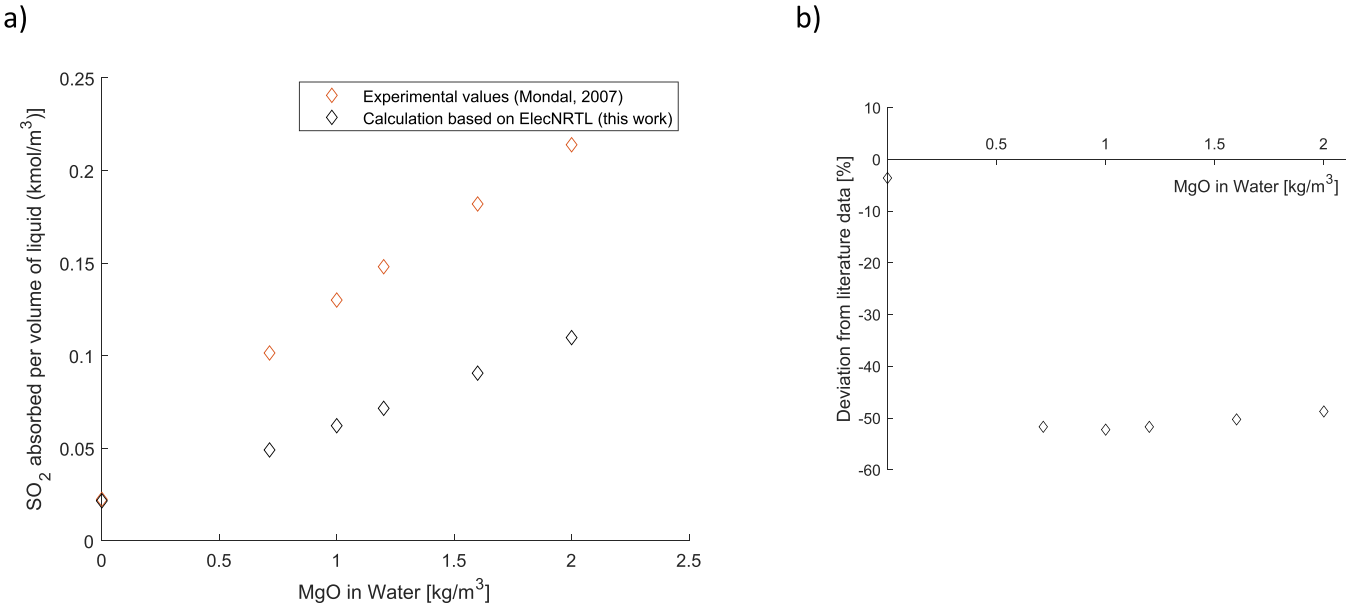

Figure 2. (a) SO_2 absorbed in $Mg(OH)_2$-H_2O solution (T = 29.85 °C, SO_2 partial pressure = 0.963 kPa).[14] (b) Deviation of calculated values from literature data (see eq 26).

https://doi.org/10.1021/acs.iecr.3c00868
Ind. Eng. Chem. Res. XXXX, XXX, XXX−XXX

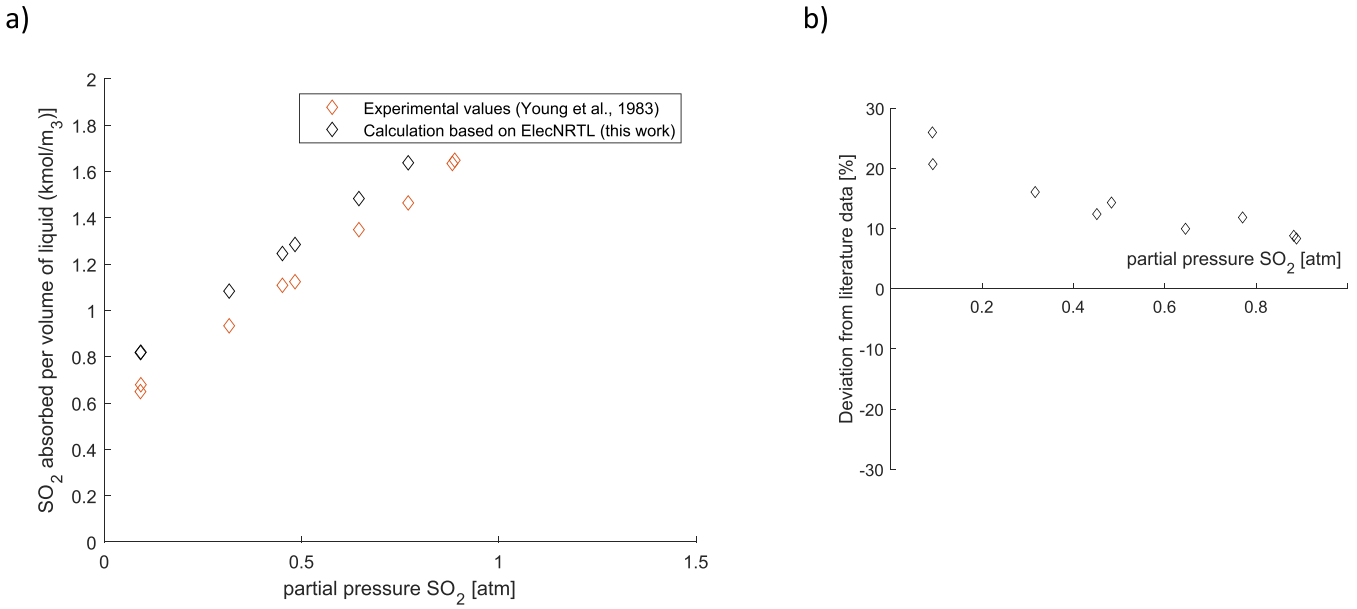

Figure 3. (a) SO_2 absorbed in $Mg(OH)_2$-H_2O solution (T = 24 °C, MgO concentration: 14.5 kg/m^3 MgO in water).[13] (b) Deviation of calculated values from literature data (see eq 26).

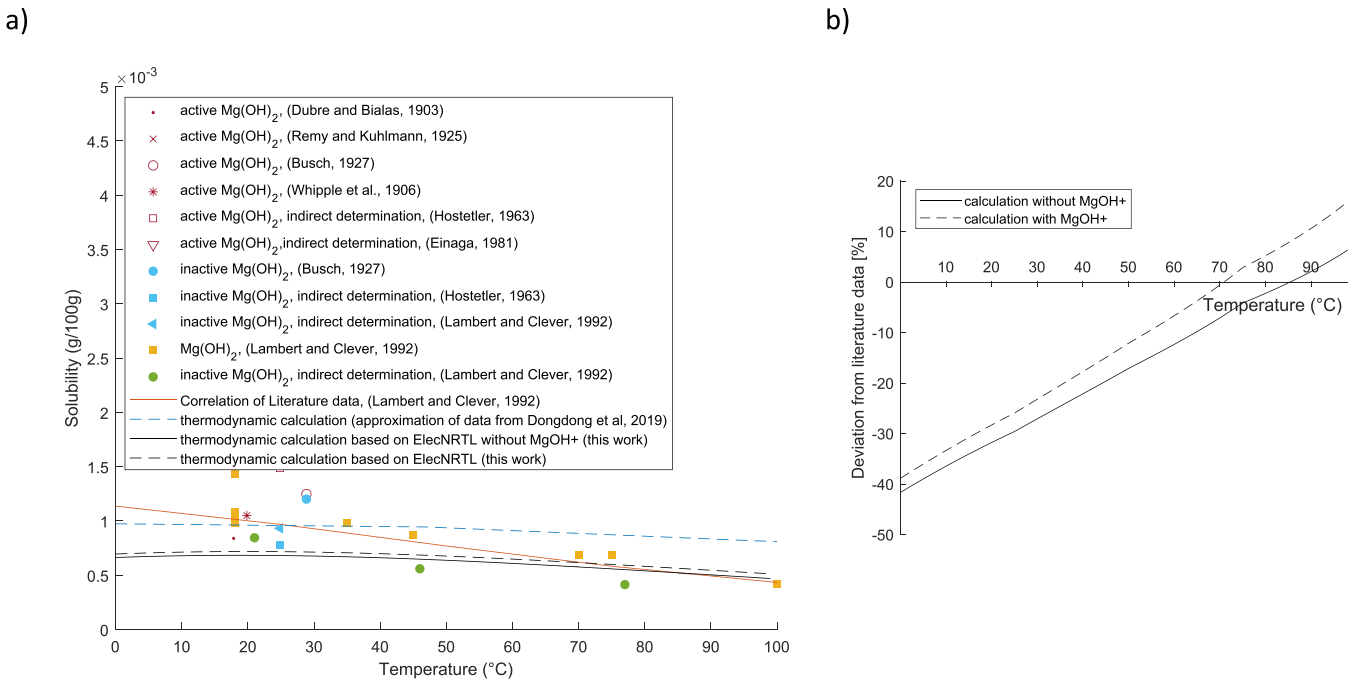

Figure 4. (a) Solubility of $Mg(OH)_2$ in water over temperature.[15−22] (b) Deviation of calculated values from the correlation of literature data by Lambert and Clever (see eq 26).

$Ca(OH)_2$, the solubility of $MgSO_3$ and $CaSO_3$ hydrates, and the solubility of $MgSO_4$ and $CaSO_4$ hydrates.

3.1. SO_2 Solubility. *3.1.1. SO_2 Solubility in Water.* Figure 1 shows the calculated SO_2 solubility in water compared with experimental data from the literature.

When calculating the solubility in water, the model shows, in general, a good agreement with the literature data. It is expected that electrolyte reactions increase the solubility of SO_2. This increase can also be observed when comparing the calculated results with and without considering electrolyte reactions. The calculated increase in solubility is around 6% at 20 °C and around 18% at 90 °C. Even if the calculation with the electrolyte reactions is the more detailed approach, the performed calculations cannot justify the necessity to implement the electrolyte reactions to calculate the SO_2 solubility in water. Compared to the newer data from Rumpf and Maurer, the calculation without electrolyte reactions performs better than the calculation with electrolyte reactions at temperatures >50 °C. Compared with the IUPAC correlation of literature data, however, the calculation with electrolyte reactions performs better at temperatures >40 °C. Considering electrolyte reactions does therefore not necessarily improve the accuracy of the calculation when compared to experimental data from the literature.

https://doi.org/10.1021/acs.iecr.3c00868
Ind. Eng. Chem. Res. XXXX, XXX, XXX−XXX

3.1.2. SO_2 Absorption in $Mg(OH)_2$ Solution. Due to the chemical absorption, the presence of $Mg(OH)_2$ increases the solubility of SO_2 significantly. Figures 2 and 3 show the calculated absorbed SO_2 compared to experimental values from the literature.

The simulation results show the same trend as the experimental values found in the literature, but the absolute values show some deviation. However, the deviation is not consistent. For low MgO concentration, as studied by Mondal,[14] the model underestimates the absorbed SO_2 by around 49 to 51% (Figure 2). Mondal derives an enhancement factor of 5 at a MgO concentration of 1 kg/m^3. The calculation leads only to an enhancement factor of 2.5. The calculated effect of the $Mg(OH)_2$ on the SO_2 absorption is, therefore, only half compared to the measured effect by Mondal.

For high MgO concentrations, as studied by Young et al. and reported in the IUPAC solubility data series, the model overestimates the absorbed SO_2[13] (Figure 3). At a low SO_2 partial pressure of 0.091 atm, the model calculates a between 20 and 26% higher absorption. At a high partial pressure of 0.888 atm, it calculates an 8% higher absorption than reported in the literature. The overestimation of the absorbed SO_2 by the model compared to the measured values could indicate that the experiment's equilibrium has not been reached. In the model calculation, it was assumed that all the MgO present in water hydrates to $Mg(OH)_2$ and takes part in the absorption reactions. However, reaching a total hydration rate in a real system is difficult. The overestimation by the model could also indicate that there was not a 100% hydration rate reached in the experimental setup. However, the present data do not deliver enough evidence for such theories. Furthermore, the contrary deviation for low MgO concentrations[14] does not support this theory either. The available experimental data are too scarce to derive a trustful evaluation of the model in this regard. Therefore, the model was not adapted to fit one of the experimental data sets.

3.2. Solubility of Magnesium Hydroxide ($Mg(OH)_2$). Figure 4 shows the calculated solubility of $Mg(OH)_2$ in water compared with data from the literature.

The calculated solubility shows very good agreement with the literature data. The trend of the calculated solubility is parallel to that of Dongdong et al. using the Calphad method[22] but reveals lower solubility values. While at a temperature around 20 to 30 °C the model predicts a lower solubility than most experimental data, the model fits the experimental data very well in the temperature range from 70 to 90 °C with a deviation close to 0%. Furthermore, the calculation shows that including the formation of the $MgOH^+$ ion pair in the calculation has little effect on the solubility of $Mg(OH)_2$. The model would therefore allow a simplification of the chemical system by disregarding the formation of $MgOH^+$. It needs to be considered that the model describes the solubility of thermodynamic stable (inactive) $Mg(OH)_2$. In real systems, $Mg(OH)_2$ can also be present as active $Mg(OH)_2$. Literature data indicate that active $Mg(OH)_2$ has a higher solubility and that the solubility decreases with aging and the transformation to inactive $Mg(OH)_2$. This might be relevant for the temperature range of 20 to 30 °C. However, literature data are not definite about this decrease.[21]

Figure 5 shows the modeled pH dependency of the solubility of $Mg(OH)_2$ and the pH dependency given by the equation of Scholz and Kahlert.[23]

The calculation shows the same trend as the trend given by Scholz and Kahlert,[23] which is the solubility drop at a specific pH value. While $Mg(OH)_2$ is very soluble at a low pH value, the solubility drops rapidly between a pH of 8 and 9. According to the model, this solubility drop happens at a pH of 8.36. According to Scholz and Kahlert's calculation, it occurs at a pH of 8.1. The pH dependency given by Scholz and Kahlert is derived from an equation to calculate the solubility as a function of pH value, solubility product taken from literature, and the acid constant of water and is not derived directly from experimental data.[23] Using Scholz and Kahlert's equation with a 5% lower solubility product, the model's calculation and the calculation following Scholz and Kahlert match very well. This shows that the underlying solubility product input can be one cause for the deviation from Scholz and Kahlert's dependency.

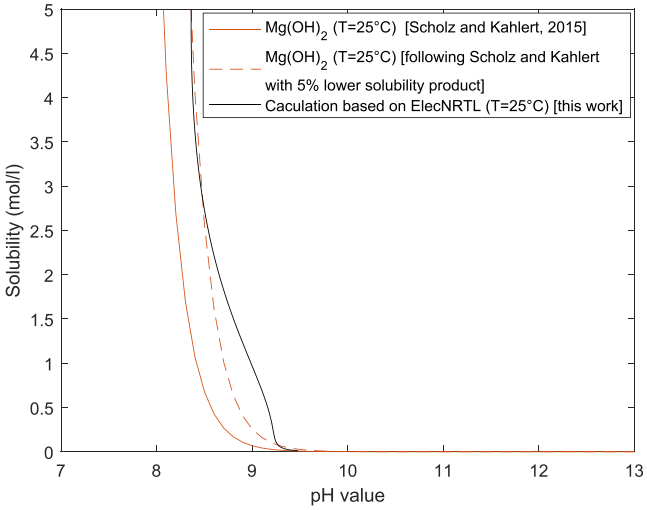

Figure 5. Solubility of $Mg(OH)_2$ depending on the pH value.[23]

3.3. Solubility of Calcium Hydroxide ($Ca(OH)_2$). Figure 6 shows the calculated solubility of $Ca(OH)_2$ in water compared with data from the literature.

The calculated solubility shows the same trend as the experimental data from the literature. Unlike for $Mg(OH)_2$, including the formation of the $CaOH^+$ ion pair in the calculation shows an improving effect on the calculated solubility of $Ca(OH)_2$. Without considering the formation of $CaOH^+$, the model underestimates the solubility by 19 to 33% compared to the correlation of Lambert and Clever.[21] Considering the formation of $CaOH^+$, the model underestimates the solubility only by around 4.5 to 11%.

Like $Mg(OH)_2$, the solubility of $Ca(OH)_2$ is strongly pH-dependent. Figure 7 shows the modeled pH dependency of the solubility of $Ca(OH)_2$ and the pH dependency given by the equation of Scholz and Kahlert.[23]

As for $Mg(OH)_2$, the solubility is very high for low pH values and drops rapidly when reaching a certain pH level. The modeled solubility drop happens at a pH value of around 11.6; using Scholz and Kahlert's equation reveals a solubility drop at a pH value of 11.1.[23] As for $Mg(OH)_2$, one reason for this deviation between the two calculated pH dependencies can be the underlying solubility product taken from the literature. Lowering the underlying solubility product in Scholz and Kahlert's equation by 17% reveals a very good match to the model calculation.

3.4. Solubility of Magnesium Sulfite ($MgSO_3$). Figure 8 shows the calculated solubility of $MgSO_3$ hydrates in water compared with data from the literature.

https://doi.org/10.1021/acs.iecr.3c00868
Ind. Eng. Chem. Res. XXXX, XXX, XXX−XXX

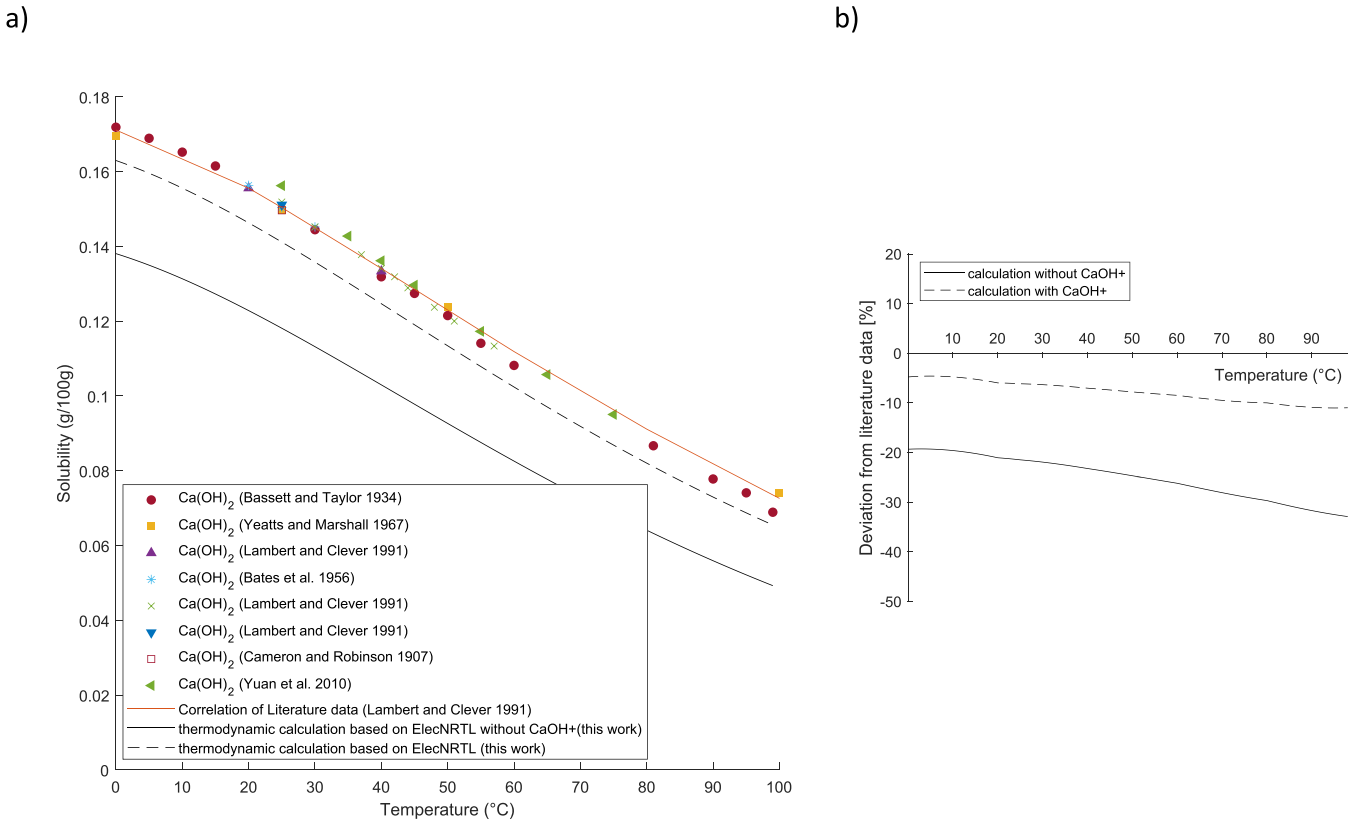

Figure 6. (a) Solubility of $Ca(OH)_2$ in water over temperature.[21,24−27] (b) Deviation of calculated values from the correlation of literature data by Lambert and Clever (see eq 26).

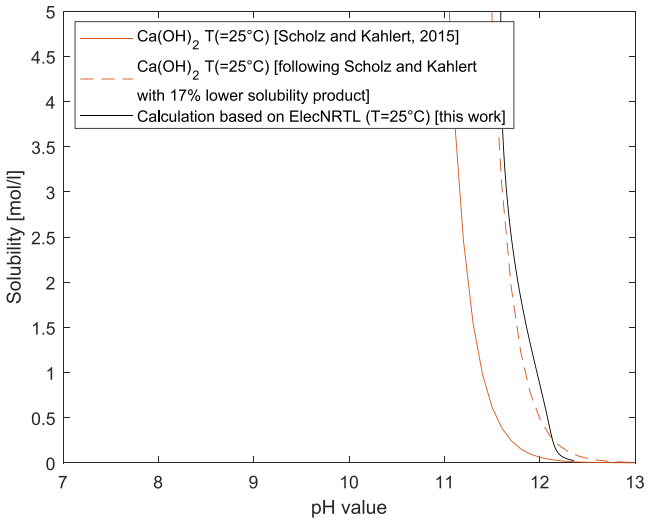

Figure 7. Solubility of $Ca(OH)_2$ depending on the pH value.[23]

The model predicts the hexahydrate as the stable form at lower temperatures and the trihydrate as the stable form at higher temperatures. This fits with the experimental data reported in the literature. When calculating the solubility of $MgSO_3$ hydrates based on the reference state Gibbs free energies, the model overestimates the hexahydrate's solubility and underestimates the trihydrate's solubility compared to the experimental data. Furthermore, the model predicts the change from hexahydrate to trihydrate as the stable hydrate form at around 12 °C. Following experimental data, this change happens at about 40 °C. This deviation between the model and experimental values is closed when calculating with the temperature-dependent equilibrium constants. The calculated solubility fits very well with the experimental data from the literature. When using the model to calculate a real system, it must be considered that it predicts the formation and solubility of the stable hydrate form at the given temperature. Therefore, at temperatures higher than 40 °C, the model reports solely the formation of $MgSO_3$ trihydrate, as this is the stable form at those temperatures. However, the conversion from hexahydrate to trihydrate can be very slow in real systems. This can lead to the co-presence of meta-stable hexahydrate at temperatures above 40 °C even though trihydrate is the stable form at this temperature.[29,31,48] The equilibrium model cannot cover the dynamic behavior of the transition from hexahydrate to trihydrate. As trihydrate has a higher solubility than hexahydrate at temperatures over 40 °C, this can lead to an overestimation of precipitates in the system when modeling the system.

Figure 9 shows the calculated solubility of $MgSO_3$ trihydrate depending on the $MgSO_4$ content in the system compared to experimental data from the literature.

The model predicts the dependency of the solubility on the $MgSO_4$ content in the solution satisfactorily. Up to a $MgSO_4$ content of 10 g/100 g, the calculated solubility lies within the deviation of the available literature data. At higher $MgSO_4$ content, the model underestimates the solubility of the trihydrate. However, the deviation compared to the data of Lutz does not exceed 30%.

Figure 10 shows the calculated solubility of $MgSO_3$ hexahydrate depending on the $MgSO_4$ content in the system compared to experimental data from the literature.

https://doi.org/10.1021/acs.iecr.3c00868
Ind. Eng. Chem. Res. XXXX, XXX, XXX−XXX

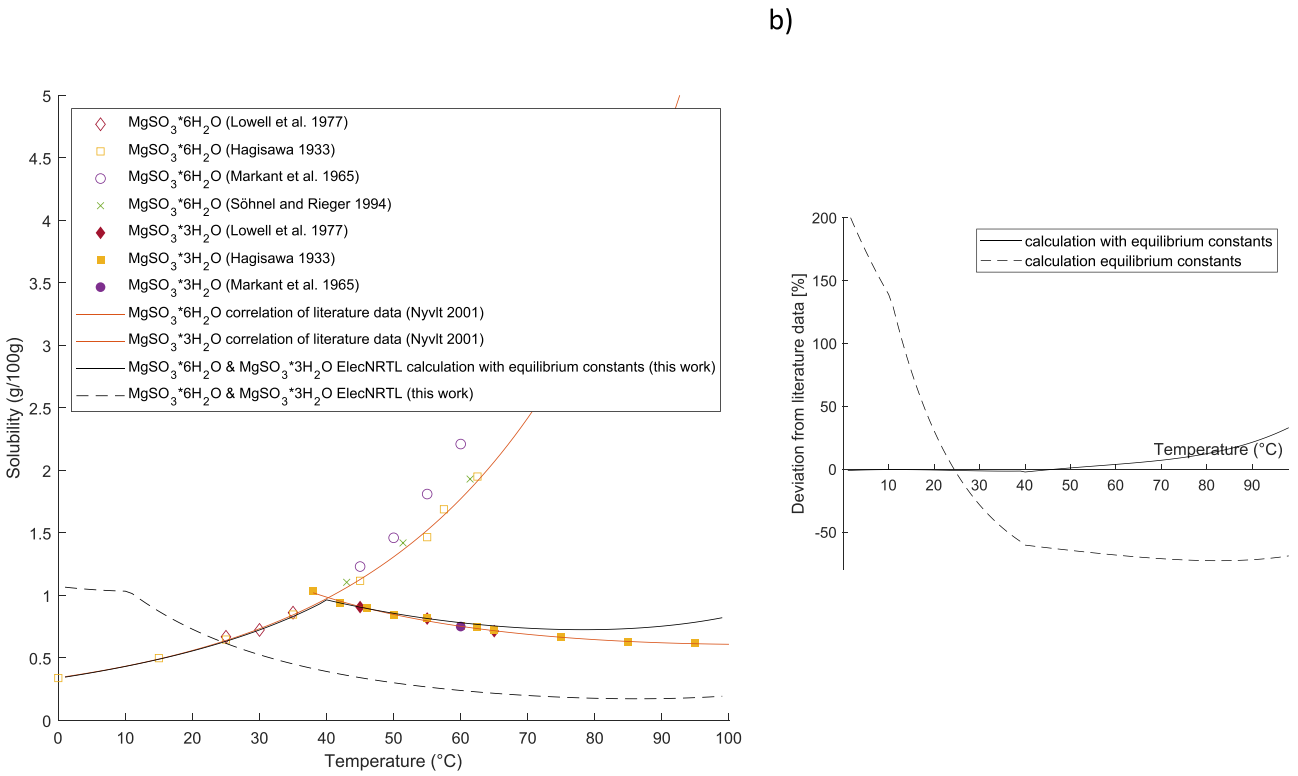

Figure 8. (a) Solubility of $MgSO_3$ hydrates in water over temperature.[28−32] (b) Deviation of calculated values from the correlation of literature data by Nývlt (see eq 26).

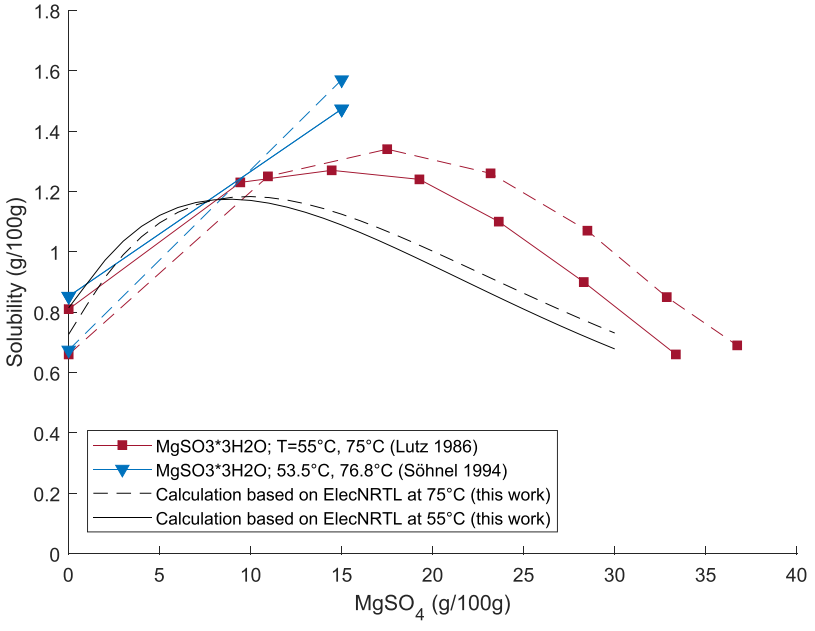

Figure 9. Solubility of $MgSO_3$ trihydrate over $MgSO_4$ content at different temperatures.[31,33]

The calculated solubility shows a similar trend as the solubility reported in literature and lies within the deviation between the different reported experimental data. As for the trihydrate, the model tends to underestimate the solubility at high $MgSO_4$ contents.

3.5. Solubility of Calcium Sulfite ($CaSO_3$). Figure 11 shows the calculated solubility of $CaSO_3$ hydrates in water compared with data from the literature.

In literature, different hydrate forms of $CaSO_3$ are reported in the temperature range from 30 to 100 °C. However, $CaSO_3$ hemihydrate is recognized as the dominant one.[33] The calculated solubility of $CaSO_3$ hemihydrate based on the reference state Gibbs free energies shows very good agreement with the correlation of literature data done by Lutz at temperatures >50 °C with a deviation of <8%.

https://doi.org/10.1021/acs.iecr.3c00868
Ind. Eng. Chem. Res. XXXX, XXX, XXX−XXX

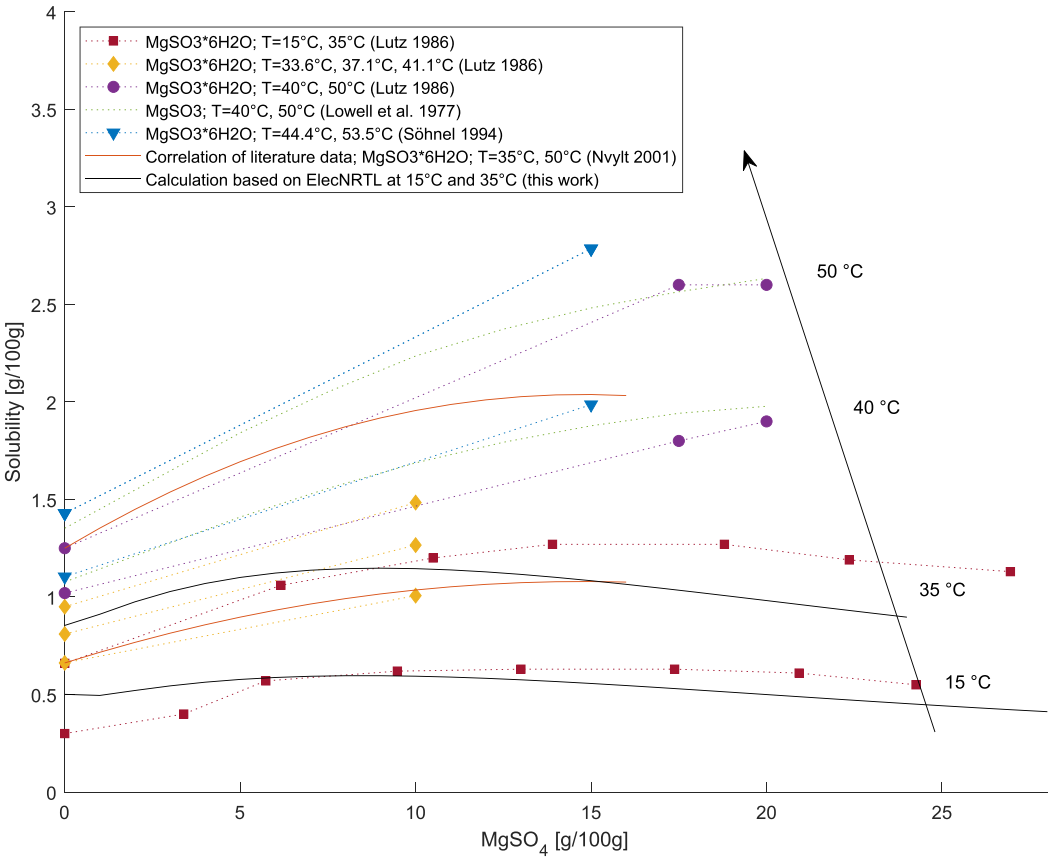

Figure 10. Solubility of $MgSO_3$ hexahydrate over $MgSO_4$ content at different temperatures.[31−33]

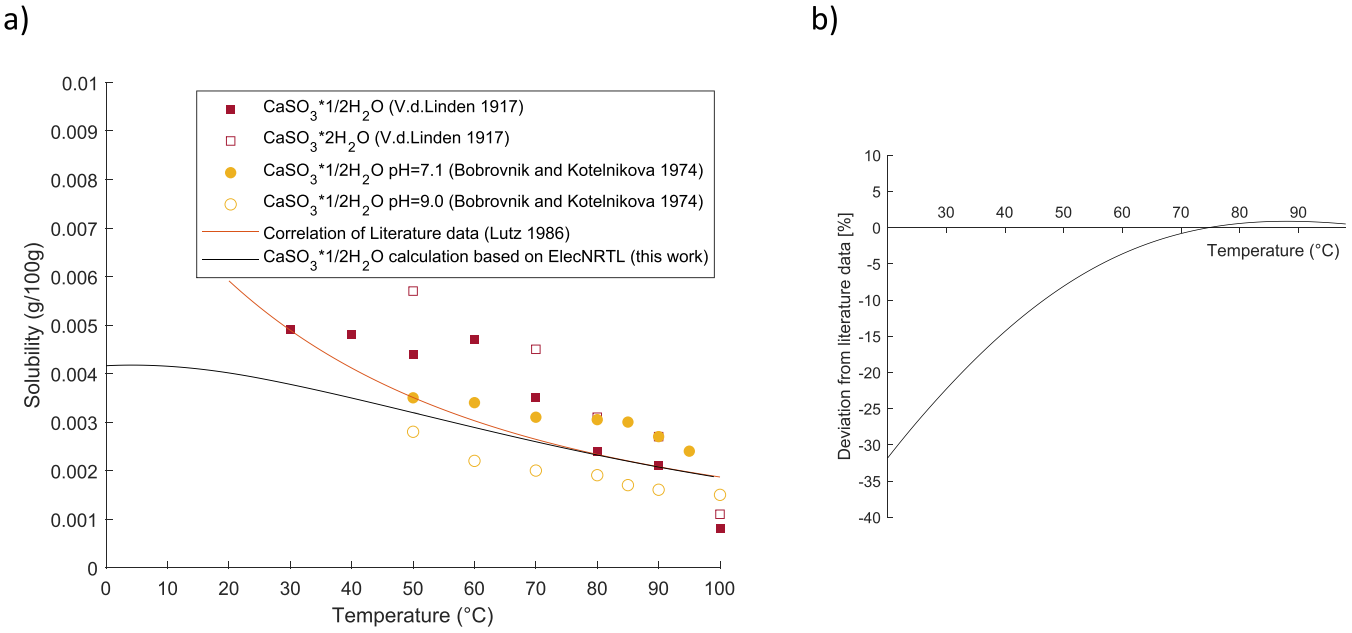

Figure 11. (a) Solubility of $CaSO_3$ hydrates in water over temperature.[33−35] (b) Deviation of calculated values from the correlation of literature data by Lutz (see eq 26).

Figure 12 shows the calculated solubility of $CaSO_3$ hemihydrate in water and a $CaSO_4$-saturated solution compared to experimental data from the literature.

The solubility of $CaSO_3$ hemihydrate is lower in the presence of $CaSO_4$. The model describes this decrease in solubility. For temperatures ≥80 °C, the model fits very well with the measured values of van der Linden. For lower temperatures, the model underestimates the solubility of $CaSO_3$ hemihydrate compared to the data from van der Linden and Lutz. This correlates with the findings from Figure 11, where the model also underestimates the solubility at lower temperatures. Bichowsky measures a lower solubility than van der Linden and Lutz.

https://doi.org/10.1021/acs.iecr.3c00868
Ind. Eng. Chem. Res. XXXX, XXX, XXX−XXX

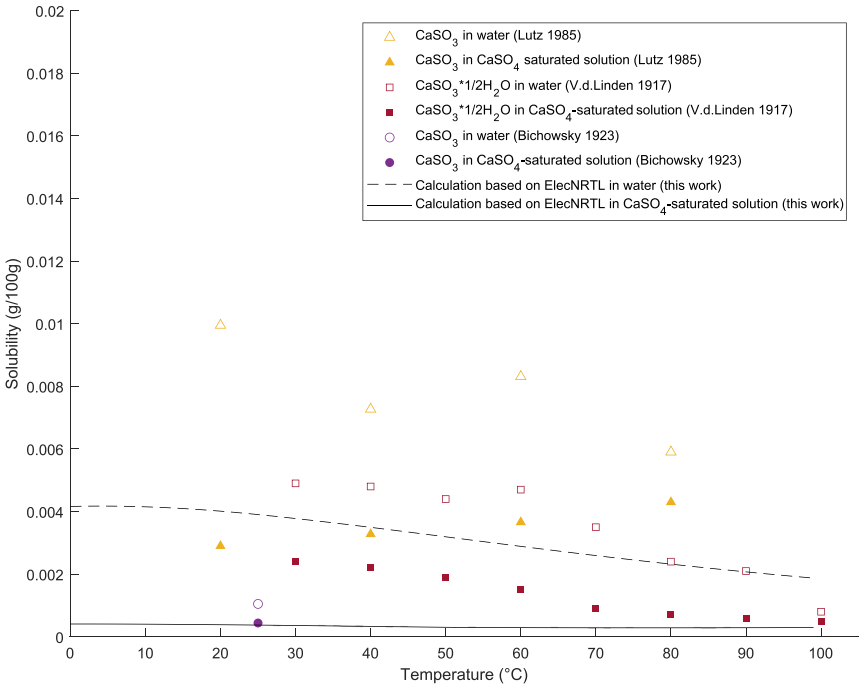

Figure 12. Solubility of $CaSO_3$ hydrates over $CaSO_4$ content at different temperatures.[33,34,36]

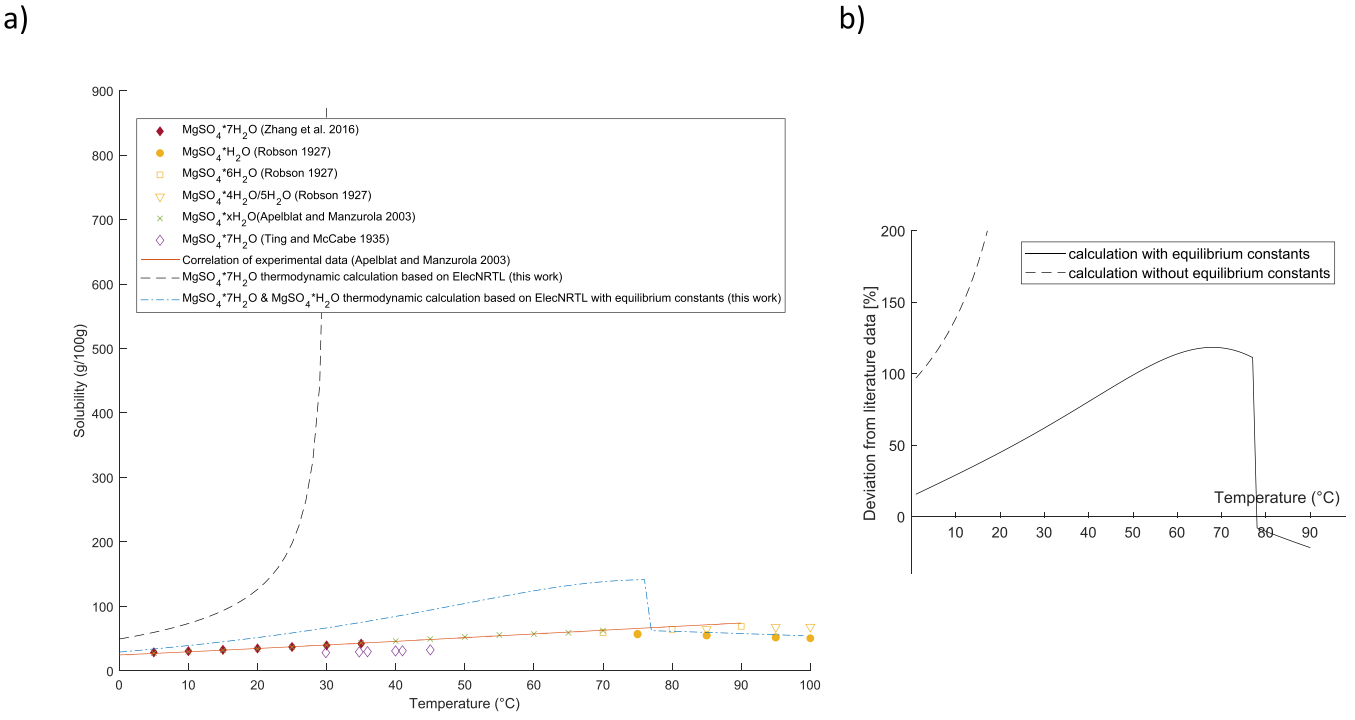

Figure 13. (a) Solubility of $MgSO_4$ hydrates in water over temperature.[37−40] (b) Deviation of calculated values from the correlation of literature data by Apelblat and Manzurola (see eq 26).

Compared to the data of Bichowsky, the model describes the solubility in $CaSO_4$-saturated solution at 25 °C very well.

3.6. Solubility of Magnesium Sulfate ($MgSO_4$). Figure 13 shows the calculated solubility of $MgSO_4$ hydrates in water over temperature compared with data from the literature.

The model recognizes only heptahydrate as the present hydrate form when calculating the solubility based on the reference state Gibbs free energies. Furthermore, the model predicts a significant increase in solubility with increasing temperatures. However, experimental data from literature show that up to 48 °C heptahydrate is the stable hydrate form, between 48 and 68 °C hexahydrate is the stable form, and monohydrate is the stable one at temperatures higher than 68 °C.[38,39] When applying the equilibrium constants, the model predicts heptahydrate and monohydrate as stable forms. The model does not recognize hexahydrate as a stable form between 48 and 68 °C. While the calculated solubility of the monohydrate fits the literature data very well, the calculated

https://doi.org/10.1021/acs.iecr.3c00868
Ind. Eng. Chem. Res. XXXX, XXX, XXX−XXX

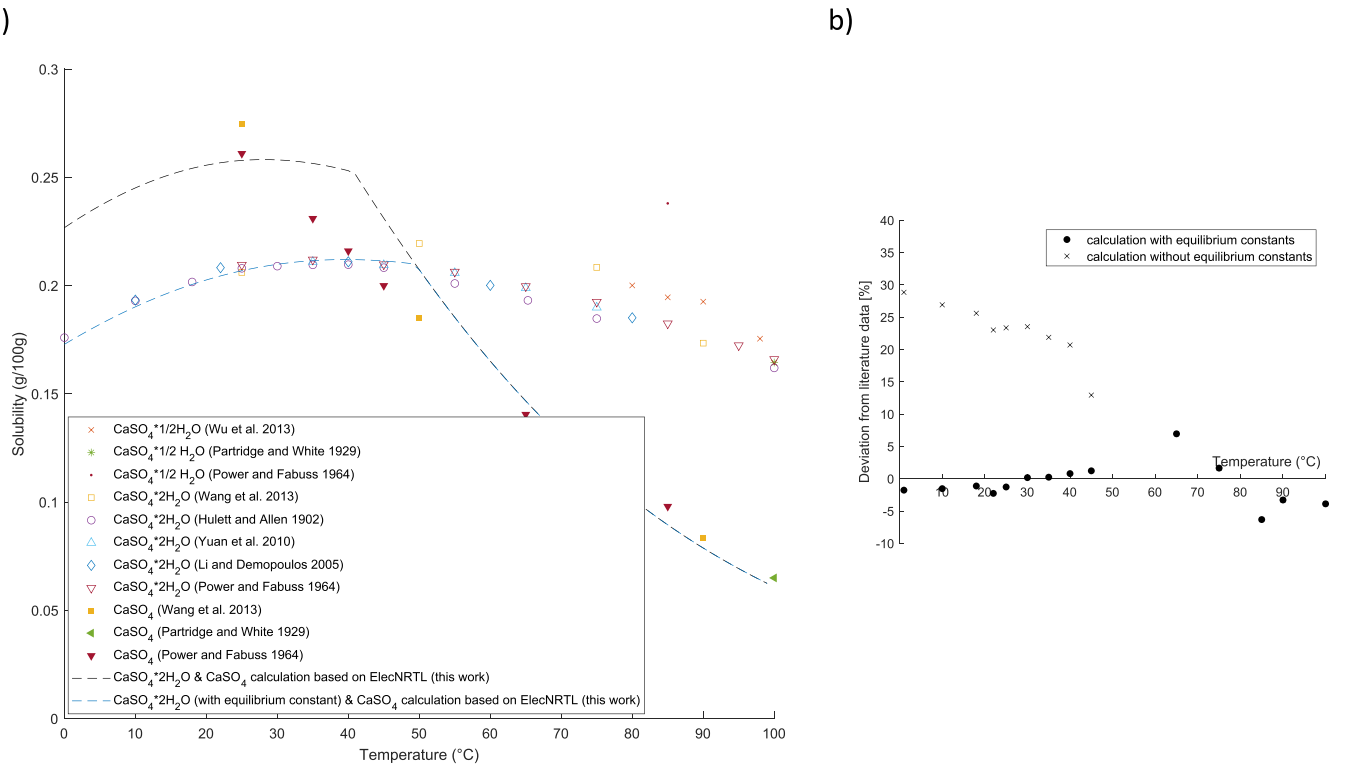

Figure 14. (a) Solubility of $CaSO_4$ hydrates in water over temperature.[41−47] (b) Deviation of calculated values from the literature data (see eq 26).

solubility of heptahydrate increases more strongly with temperature than reported in literature. This effect and the fact that hexahydrate is not recognized lead to a significant overestimation of the solubility of up to 118% at a temperature of 70 °C. The experimental solubility data for hexahydrate are scarce, which makes a consistent adaption of the model difficult.

3.7. Solubility of Calcium Sulfate ($CaSO_4$). Figure 14 shows the calculated solubility of $CaSO_4$ hydrates in water over temperature compared with data from the literature.

Experimental data from the literature report the dihydrate as a stable form at temperatures up to around 50 °C. At higher temperatures, the stable form is the anhydrate. The model describes this change in the stable hydrate form very well. When calculating the solubility based on the reference state Gibbs free energies, the model describes the solubility of the anhydrate very well and overestimates the solubility of the dihydrate. The calculated solubility of the dihydrate is improved by applying equilibrium constants for its precipitation reaction.

4. CONCLUSIONS

The electrolyte NRTL activity coefficient model was applied to model the vapor, liquid, and solid phases of the MgO-CaO-CO_2-SO_2-H_2O-O_2 system.

To model the SO_2 solubility in water, the study suggests that a simplification of the model to a simple vapor−liquid equilibrium calculation using Henry's law is possible without sacrificing model accuracy. When calculating the SO_2 absorption into $Mg(OH)_2$ slurry, considering the electrolyte reaction equilibrium is crucial. The model calculates the absorption trend correctly but shows quantitative deviations from available experimental data from the literature. However, experimental data sets for the SO_2 absorption in $Mg(OH)_2$ in literature are scarce and the evaluation of the model using available data is inconclusive on whether deviations are caused by measurement uncertainties or model parameters. More experimental data are necessary for a trustful evaluation of the model and a potential adaptation of model parameters.

The model predicts potential stable precipitates in the system at a temperature range from 0 to 100 °C correctly. The study shows that the chemical equilibrium of the precipitation of $Mg(OH)_2$, $Ca(OH)_2$, $CaSO_3$ hemihydrate, and $CaSO_4$ anhydrate can be calculated satisfactorily from the reference state Gibbs free energies of the participating components. The chemical equilibrium of the precipitation of $MgSO_3$ hexahydrate and trihydrate, $MgSO_4$ monohydrate and heptahydrate, and $CaSO_4$ dihydrate requires built-in or user-supplied parameters to describe the equilibrium constants K_{eq} as a function of temperature to achieve high accuracy of the model. The model overestimates the solubility of $MgSO_4$ heptahydrate. Due to its high solubility, $MgSO_4$ is not a critical precipitate in the system. This leads the authors to the conclusion that the model is applicable to simulate precipitation in the system even though the solubility of $MgSO_4$ heptahydrate is overestimated.

The study shows that the model describes the chemical system in equilibrium satisfactorily and is a valuable tool for predicting precipitates in the system. However, it must be considered that the model cannot cover the dynamic behavior of hydrate transition and metastability of possible precipitates in fast-changing and unstable systems.

AUTHOR INFORMATION

Corresponding Author

Bahram Haddadi − *Institute of Chemical, Environmental and Bioscience Engineering, TU Wien, 1060 Vienna, Austria;* orcid.org/0000-0003-3403-6346; Email: bahram.haddadi@tuwien.ac.at

https://doi.org/10.1021/acs.iecr.3c00868
Ind. Eng. Chem. Res. XXXX, XXX, XXX−XXX

Authors

Barbara D. Weiß − *Competence Center CHASE GmbH, 1030 Vienna, Austria; Institute of Chemical, Environmental and Bioscience Engineering, TU Wien, 1060 Vienna, Austria;* orcid.org/0000-0002-5138-3721

Michael Harasek − *Institute of Chemical, Environmental and Bioscience Engineering, TU Wien, 1060 Vienna, Austria;* orcid.org/0000-0002-6490-5840

Complete contact information is available at: https://pubs.acs.org/10.1021/acs.iecr.3c00868

Notes

The authors declare no competing financial interest.

■ ACKNOWLEDGMENTS

The authors specially thank Walter Wukovits of the Institute of Chemical, Environmental and Bioscience Engineering at TU Wien for the support in process simulation and the use of Aspen Plus. This work was financially supported by the Competence Center CHASE GmbH. CHASE Competence Center is subsidized in the frame of COMET − Competence Centers for Excellent Technologies by BMVIT, BMWFW, Wirtschaftsagentur Wien, State of Upper Austria, and its scientific partners. The COMET program is handled by FFG. The support by the project partner Sappi Papier Holding GmbH is greatly acknowledged.

■ NOMENCLATURE

A_φ	Debye−Hückel parameter
F_p	Poynting factor
G	Gibbs energy
H	Henry's constant
I_x	ionic strength (mole fraction scale)
K	equilibrium constant
M	molecular weight
N_A	Avogadro's number
Q_e	electron charge
R	gas constant
T	temperature
V	volume
Z	compressibility factor
a_{ij}, b_{ij}, c_{ij}, d_{ij}, e_{ij}, f_{ij}	unsymmetric binary parameters
a, a_i	attraction coefficient, attraction coefficient of pure component i
b, b_i	limiting volume coefficient, limiting volume coefficient of pure component i
d	mass density
f	fugacity
k	Boltzmann constant
n	mole number
p	pressure
p_i	vapor pressure of pure component i
r_i	born radius of the ionic species i
x	mole fraction in the liquid phase
y	mole fraction in the vapor phase
z_i	charge number of ion i

Greek symbols

φ	fugacity coefficient
ε	dielectric constant
α_{ij}	non randomness factor
ρ	"closest approach" parameter (following Pitzer set to 14.9)
τ_{ij}	energy parameter
γ	activity coefficient

Subscripts

i	component i
m	molar
c	critical
s	solvent
w	water

Superscripts

v	vapor phase
l	liquid phase
∞	infinite dilution
*	reference state
E	excess

■ REFERENCES

(1) Zou, Y.; Liu, X.; Zhu, T.; Tian, M.; Cai, M.; Zhao, Z.; Wu, H. Simultaneous Removal of NO x and SO2 by MgO Combined with O3 Oxidation: The Influencing Factors and O3 Consumption Distributions. *ACS Omega* **2019**, *4*, 21091−21099.

(2) Steindl, M.; Röder, T.; Simharl, R.; Harasek, M.; Friedl, A.; Sixta, H. Online Raman monitoring of the phase transition of magnesium sulphite hydrate. *Chem. Eng. Process.: Process Intesif.* **2005**, *44*, 471−475.

(3) Si, T.; Wang, C.; Yan, X.; Zhang, Y.; Ren, Y.; Hu, J.; Anthony, E. J. Simultaneous removal of SO2 and NOx by a new combined spray-and-scattered-bubble technology based on preozonation: From lab scale to pilot scale. *Appl. Energy* **2019**, *242*, 1528−1538.

(4) Schöggl, K.; Steindl, M.; Friedl, A.; Weber, H. K.; Sixta, H. Calculation of physical property data of the system MgO-SO2_H2O and their implementation in Aspen Plus. *Lenzinger Berichte* **2006**, *86*, 56−62.

(5) Zidar, M.; Golob, J.; Veber, M.; Vlachy, V. Absorption of SO2 into Aqueous Solutions. 2. Gas−Liquid Equilibrium of the MgO−SO2−H2O System and Graphical Presentation of Operation Lines in an Equilibrium Diagram. *Ind. Eng. Chem. Res.* **1997**, *36*, 4342−4346.

(6) Pasiuk-Bronikowska, W.; Rudzinski, K. J. Absorption of SO2 into aqueous Systems. *Chem. Eng. Sci.* **1991**, *46*, 2281−2291.

(7) Weiß, B. D.; Harasek, M. Solubility Data of Potential Salts in the MgO-CaO-SO2-H2O-O2 System for Process Modeling. *Processes* **2021**, *9*, 50.

(8) Chen, C.-C.; Evans, L. B. A local composition model for the excess Gibbs energy of aqueous electrolyte systems. *AIChE J.* **1986**, *32*, 444−454.

(9) Mock, B.; Evans, L. B.; Chen, C.-C. Thermodynamic representation of phase equilibria of mixed-solvent electrolyte systems. *AIChE J.* **1986**, *32*, 1655−1664.

(10) Redlich, O.; Kwong, J. N. S. On the thermodynamics of solutions; an equation of state; fugacities of gaseous solutions. *Chem. Rev.* **1949**, *44*, 233−244.

(11) Sanku, M. G.; Svensson, H. Modelling the precipitating non-aqueous CO2 capture system AMP-NMP, using the unsymmetric electrolyte NRTL. *Int. J. Greenhouse Gas Control* **2019**, *89*, 20−32.

(12) Rumpf, B.; Maurer, G. Solubilities of hydrogen cyanide and sulfur dioxide in water at temperatures from 293.15 to 413.15 K and pressures up to 2.5 MPa. *Fluid Phase Equilib.* **1992**, *81*, 241−260.

(13) Young, C. L.; Gerrard, W.; Battino, R. Sulfur Dioxide, Chlorine, Fluorine and Chlorine Oxides. *Solubility Data Ser.* **1983**, *12*, 4−77.

(14) Mondal, M. K. Absorption equilibria of dilute sulphur dioxide in Mg(OH)2 slurry. *Fluid Phase Equilib.* **2007**, *262*, 111−120.

(15) Dupré; Bialas, J. Zur Bestimmung der Löslichkeit von Magnesia und Zinkoxyd in Wasser auf Grund des elektrischen Leitvermögens. *Z. Angew. Chem.* **1903**, *16*, 54−55.

(16) Remy, H.; Kuhlmann, A. Löslichkeitsbestimmungen an schwer löslichen Stoffen. II. Wasserlöslichkeit der Oxyde von Beryllium, Aluminium, Zink, Cadmium, Blei, Kupfer und Silber. *Fresenius, Zeitschrift f. anal. Chemie* **1924**, *65*, 161−181.

(17) Busch, W. Über die Verwendbarkeit der elektrometrischen Titration zur Löslichkeitsbestimmung schwerlöslicher Oxyde. *Zeitschrift für anorganische und allgemeine Chemie* **1927**, *161*, 161−179.
(18) Whipple, G. C.; Mayer, A. The Solubility of Calcium Carbonate and of Magnesium Hydroxide and the Precipitation of These Salts with Lime Water. *J. Infect. Dis.* **1906**, *3*, S151−S165.
(19) Hostetler, P. B. The stability and surface energy of brucite in water at 25 degrees C. *Am. J. Sci.* **1963**, *261*, 238−258.
(20) Einaga, H. The hydrolytic precipitation reaction of Mg(II) from aqueous NaNO3 solution. *J. Inorg. Nucl. Chem.* **1981**, *43*, 229−233.
(21) Lambert, I.; Clever, H. L. Alkaline Earth Hydroxides in Watern and aqueous solutions. *Solubility Data Ser.* **1992**, *52*, 49−226.
(22) Dongdong, L.; Dandan, G.; Yaping, D.; Wu, L. Modeling of phase relations and thermodynamics in the Mg(OH)2 + MgSO4 + H2O system with implications on magnesium hydroxide sulfate cement. *Calphad* **2019**, *67*, No. 101675.
(23) Scholz, F.; Kahlert, H. The calculation of the solubility of metal hydroxides, oxide-hydroxides, and oxides, and their visualisation in logarithmic diagrams. *ChemTexts* **2015**, *1*, 1−9.
(24) Bassett, H.; Taylor, H. S. CLXXX.—Calcium nitrate. Part III. The three-component system: calcium nitrate−lime−water. *J. Chem. Soc., Trans.* **1914**, *105*, 1926−1941.
(25) Yeatts, L. B.; Marshall, W. L. Aqueous systems at high temperature. XVIII. Activity coefficient behavior of calcium hydroxide in aqueous sodium nitrate to the critical temperature of water. *J. Phys. Chem.* **1967**, *71*, 2641−2650.
(26) Bates, R. G.; Bower, V. E.; Smith, E. R. Calcium hydroxide as a highly alkaline pH standard. *J. Res. Natl. Bur. Stand* **1956**, *56*, 305.
(27) Cameron, F. K.; Robinson, W. O. The System, Lime, Nitric Acid and Water. *J. Phys. Chem.* **1907**, *11*, 273−278.
(28) Lowell, P. S.; Meserole, F. P.; Parsons, T. B. *Preciptiation Chemistry of Magnesium Sulfite Hydrates in Magnesium Oxide Scrubbing*. Interagency Energy-Environment Research and Development series 1977, EPA-600/7−77-109 (EPA-600/7−77-109).
(29) Hagisawa, H. Studies of Magnesium Sulphite. *Bull. Inst. Phys. Chem. Res.* **1933**, *12*, 976−983.
(30) Markant, H. P.; McIlroy, R. A.; Matty, R. E. Absorption Studies - MgO-SO2 Systems. *Tappi* **1962**, *45*, 849−854.
(31) Söhnel, O.; Rieger, A. Solubilites of Magnesium Sulfite Hydrates. *J. Chem. Eng. Data* **1994**, *39*, 161−162.
(32) Nývlt, J. Solubilities of Magnesium Sulfite. *J. Therm. Anal. Calorim.* **2001**, *66*, 509−512.
(33) Lutz, H. D. Sulfites, Selenites and Tellurites. *Solubility Data Ser.* **1986**, *26*, 153−193.
(34) van der Linden, T. Solubility of calcium sulphite in water and in sugar solutions. *J. Chem. Technol. Biotechnol.* **1917**, *36*, 96.
(35) Bobrovnik, L. D.; Kotelnikova, L. P. Solublity of calcium sulphite in sugar solutions. *Izv. Vyssh. Uchebn. Zaved., Pishch. Tekhnol.* **1974**, *4*, 155−156.
(36) Bichowsky, F. R. FREE ENERGY OF THE THIOSULFATE ION. *J. Am. Chem. Soc.* **1923**, *45*, 2235.
(37) Zhang, Y.; Asselin, E.; Li, Z. Solubility Measurement and Chemical Modeling of MgSO 4 ·7H 2 O in the Ti(SO 4) 2 −H 2 SO 4 −H 2 O System. *J. Chem. Eng. Data* **2016**, *61*, 2363−2370.
(38) Robson, H. L. THE SYSTEM MgSO 4 -H 2 O FROM 68 TO 240° 1. *J. Am. Chem. Soc.* **1927**, *49*, 2772−2783.
(39) Apelblat, A.; Manzurola, E. Solubilites and vapour pressures of saturated aqueous solutions of sodium tetraborate, sodium carbonate, and magnesium sulfate at freezing-temperature lowerings of sodium tetraborate and sodium carbonate solutions. *J. Chem. Thermodyn.* **2003**, *35*, 221−238.
(40) Ting, H. H.; McCabe, W. L. Solubility of Magnesium Sulfate Heptahydrate. *Ind. Eng. Chem.* **1934**, *26*, 1207−1208.
(41) Wu, X.; Wang, K.; Xiong, Z.; Ye. Solubility of α-Calcium Sulfate Hemihydrate in Ca−Mg−K Chloride Salt Solution at (353.0 to 371.0) K. *J. Chem. Eng. Data* **2013**, *58*, 48−54.
(42) Partridge, E. P.; White, A. H. THE SOLUBILITY OF CALCIUM SULFATE FROM 0 TO 200°. *J. Am. Chem. Soc.* **1929**, *51*, 360−370.
(43) Power, W. H.; Fabuss, B. M. Transient Solubilities in the Calcium Sulfate-Water System. *J. Chem. Eng. Data* **1964**, *9*, 437−442.
(44) Wang, W.; Zeng, D.; Chen, Q.; Yin, X. Experimental determination and modeling of gypsum and insoluble anhydrite solubility in the system CaSO4−H2SO4−H2O. *Chem. Eng. Sci.* **2013**, *101*, 120−129.
(45) Hulett, G. A.; Allen, L. E. THE SOLUBILITY OF GYPSUM. *J. Am. Chem. Soc.* **1902**, *24*, 667−679.
(46) Yuan, T.; Wang, J.; Li, Z. Measurement and modelling of solubility for calcium sulfate dihydrate and calcium hydroxide in NaOH/KOH solutions. *Fluid Phase Equilib.* **2010**, *297*, 129−137.
(47) Li, Z.; Demopoulos, G. P. Solubility of CaSO 4 Phases in Aqueous HCl + CaCl 2 Solutions from 283 K to 353 K. *J. Chem. Eng. Data* **2005**, *50*, 1971−1982.
(48) Söhnel, O.; Rieger, A. Phase Transition of Magnesium Sulphite Hydrates in Aqueous Suspension. *Cryst. Res. Technol.* **1993**, *28* (4), 487−493.

https://doi.org/10.1021/acs.iecr.3c00868
Ind. Eng. Chem. Res. XXXX, XXX, XXX−XXX